

REGIONAL CEREBRAL BLOOD FLOW

WITH THE ANGER CAMERA

B. Leonard Holman, Rex Hill, David O. Davis, and E. James Potchen

*Edward E. Mallinckrodt Institute of Radiology,
Washington University School of Medicine, St. Louis, Missouri*

In the past several years there has been considerable interest in measuring regional blood flow. In particular the cerebral circulation has been under intensive study in an effort to unravel the physiologic bases of cerebral hemodynamics and to improve the therapeutic management of cerebrovascular disease (1-3).

We have developed a method for quantifying regional cerebral blood flow (rCBF) with the Anger camera interfaced with a small general-purpose computer. The scintillation camera has several practical advantages: (A) It is commonly available in most major medical centers; (B) the thin crystal is suitable for the detection of low-energy photons from nuclides such as ^{133}Xe ; (C) the camera output is easily interfaced to a computer for data accumulation, storage, and processing; and (D) the camera crystal covers the entire field of interest.

After evaluating instrumental performance, five angiographically normal patients were studied. This paper describes the methodology and critically evaluates the technique. The biological data are analyzed and compared with data derived by other methods.

MATERIALS AND METHODS

Theory. Several methods have been proposed for calculating rCBF in cubic centimeters per minute per 100 grams (4-7). One of these, compartmental analysis, assumes that blood and tissue concentrations are always in equilibrium and that the brain is made of a number of parallel first-order compartments. It is doubtful whether first-order compartments are an exact representation of the frequency function of transit times through most parts of the circulatory system (8). A stochastic (height/area) method which offers a more general treatment that is not dependent on tissue homogeneity or first-order compartments has been proposed by Zierler (8). The only constraints placed on this method of anal-

ysis require that the tracer must not be metabolized or sequestered and the frequency function of transit times should not change during the time of monitoring. (These constraints are also placed on compartmental analysis.) The stochastic method has other advantages: the computer program is relatively simple and data accumulation and processing can be performed by a small general-purpose computer.

Zierler has shown that $H/A = 1/\bar{t} = F/V$, where H is the maximum height of the washout curve, \bar{t} is the mean transit time, A is the area under the curve, F is the rate of flow throughout the system, and V is the volume of the system (7,8). This formulation holds not only for an intravascular volume but also for the volume obtained when the tracer is introduced at a constant rate and is allowed to distribute between the intravascular volume V and the extravascular volume V_1 according to its steady-state concentration. Consequently, the intravascular volume is related to the extravascular volume by the partition coefficient, λ . Thus, $V = \lambda V_1$ and $H/A = F/V = F/\lambda V_1$ (9). Because the chemical affinities of blood and brain tissue are not the same, the partition coefficient (λ) must be included in the calculation in order to yield a quantitative measure of blood flow.

The washout study was terminated at 10 min for practical and historical reasons. Evidence suggests that this results in approximately a 10% overestimation of blood flow (10). Comparison between values obtained by stochastic analysis and blood flow measurements obtained by ^{85}Kr desaturation (the Kety-Schmidt method) (4) are quite close when both techniques use a 10-min cutoff (11).

These calculations and assumptions lead to the

Received Apr. 22, 1972; revision accepted July 20, 1972.

For reprints contact: B. L. Holman, Dept. of Radiology, Harvard Medical School, 25 Shattuck St., Boston, Mass. 02115.

following equation for the calculation of blood flow per tissue weight:

$$F \text{ (cc/min/100 gm)} = \frac{(H_{\text{max}} - H_{10})}{A} \times \lambda \times 100.$$

H_{max} is the maximum height of the washout curve, H_{10} is the height at 10 min, A is the area under the curve, and λ is the blood-tissue partition coefficient.

Physical properties of ^{133}Xe . The gamma-ray of ^{133}Xe gives rise to a Compton edge which is very close to the 81-keV photopeak. As a result, Compton scatter cannot effectively be eliminated from the primary photopeak without sharply reducing sensitivity. We determined the effects of the window setting of the pulse-height analyzer on resolution and sensitivity by examining scintiphotos of a standard thyroid phantom filled with ^{133}Xe in saline and placed at the collimator surface. No appreciable difference in resolution was seen on the scintigraphs resulting from an offset window or symmetric 15, 20, and 25% windows. As a result, a 25% window centered on the 81-keV photopeak was used for this study. With this setting approximately 20% of the total counts within the energy window result from scattered radiation (12).

Biological properties of ^{133}Xe . ^{133}Xe is an inert gas with high lipid solubility and small molecular size. Consequently, diffusion across the capillary endothelium is rapid and not diffusion-limited. Xenon also passes readily into the pulmonary alveoli. As a result more than 95% of the gas injected into the systemic circulation is exhaled through the lungs during the first circulation, eliminating the need for recirculation corrections (13,14).

The high lipid solubility poses problems. The solubility ratio between blood and the tissue of interest depends on the lipid content of the tissue. Consequently, the values arrived at experimentally from normal tissue may be quite different for abnormal brain depending on the lipid content of the pathological area. Because we studied angiographically normal patients, we used the normal values for λ given by Veall and Mallett (15) which were obtained from homogenized brain and whole blood. Because of the relatively high affinity between ^{133}Xe and hemoglobin, the value of λ varies considerably depending on the hematocrit of the patient. The partition coefficients for white and gray matter differ substantially because of differences in lipid content. By homogenizing an entire hemisphere, Veall and Mallett determined the mean partition coefficient ($\bar{\lambda}$) based on a 60:40 ratio of gray to white matter (15).

Technique. A 1.2-mm Davis Teflon catheter* was

* Cerebral Catheter System, DCS-2, Cook, Inc., Bloomington, Ind.



FIG. 1. Scintiphoto obtained after injection of ^{133}Xe into internal carotid artery during 10-min washout. Activity is seen in jugular vein following washout and in distribution of internal carotid artery. Left border is anterior.

inserted into the common carotid artery and positioned in the internal carotid artery. Routine cerebral angiography was performed. Patients with normal carotid angiograms were then transported to the division of nuclear medicine with the catheter in place in the internal carotid artery.

The patients were positioned under a Pho/Gamma III scintillation camera for a lateral view. The collimator was placed flush against the patient's head and parallel to the sagittal plane with the center of the crystal 2 cm above the external auditory meatus. At least 40 min were allowed to elapse between the last injection of contrast and the injection of ^{133}Xe , allowing sufficient time for the effects of the contrast on cerebral blood flow to become negligible (12).

A bolus of 5–10 mCi of ^{133}Xe dissolved in 2–4 cc of sterile pyrogen-free saline was injected rapidly through the catheter into the internal carotid artery. A scintiphoto obtained during the initial phase of the washout represented the distribution of ^{133}Xe after the injection (Fig. 1). An 8×8 grid representing the 8×8 matrix array (see section on interface and computer processing) and reduced in scale to correspond to the Polaroid image was superimposed over the scintiphoto. The regional blood flow measurements were then correlated with the anatomy and cerebral angiogram.

Detection and collimation. The ^{133}Xe washout was monitored by an unmodified Pho/Gamma III scintillation camera with a 250-keV, 4,000-hole straight-bore collimator. A 25% energy window for the pulse-height analyzer was peaked over the 81-keV

photopeak, the equivalent of a 70–90-keV window setting.

Interface and computer processing. The interface between the gamma camera and the small stored-program computer has been described in detail (16–18) and only a summary of interface considerations is given here (Fig. 2). The Anger camera output consisted of three pulses for each photon processed. Two signals represented the x and y coordinates of the scintillation within the camera crystal; the third announced to the interface the arrival of a pulse-height accepted event. The interface converted the X and Y signal levels to digital information that could be stored and processed in the computer. In order to do this within the memory of the computer, preprocessing was necessary. The 10-min examination was divided into 40 time intervals. Within each interval, data were further subdivided into a two-dimensional array of cells (representing the 64 matrix units) to provide spatial information. Each photon processed by the camera was added to the counts within the appropriate location in the computer memory, producing a two-dimensional histogram of activity for each time frame.

The interface with the camera consisted of two signal conditioning units and two analog-to-digital converters*, one for each axis. The interface was designed with considerable flexibility to allow a variety of applications and, for our purposes, was con-

nected to produce an 8×8 array covering a circumscribed square on the 10-in.-diam camera field of view (Fig. 3).

The programmed console computer (PC) developed at the Biomedical Computer Laboratory of Washington University for application in radiation treatment planning was used for data accumulation. It has a core store of 4,096 12-bit words and the memory cycle time is $3.1 \mu\text{sec}$. After completion of the washout study, the raw data were transmitted to an IBM 360/50 for processing. Recent acquisition of a PDP-12 computer with a core memory sufficiently large to handle both data accumulation and processing eliminates the need for data transfer to the IBM 360/50 and expedites data analysis after completion of the study.

Both deadtime and background corrections were performed on collected data. Of the 40 time frames used for the 10-min study, the first 20 were for 0.5 sec, the next 10 were for 10 sec, and the final 10 were for 50 sec. The early portion of the washout curve was divided into very short time frames to eliminate the early intravascular non-nutritional spike (Fig. 4). In normal areas containing large vascular structures (i.e., the internal carotid artery bifurcation), the injected bolus of ^{133}Xe created an artifactually high maximum height of the washout curve (H_{max}). This was due to intravascular transit before the xenon diffused into the brain parenchyma (12). This phenomenon has also been seen overlying regions of cerebral pathology (19). If longer time frames had been used, this spike would have been

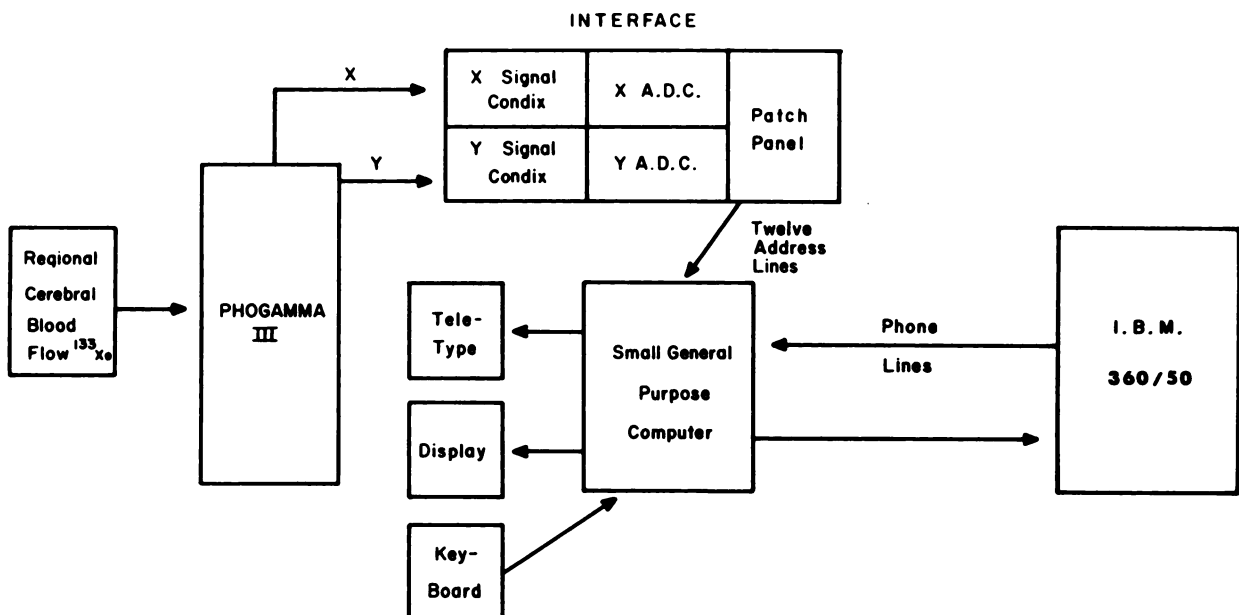


FIG. 2. Block diagram of data storage and processing system.

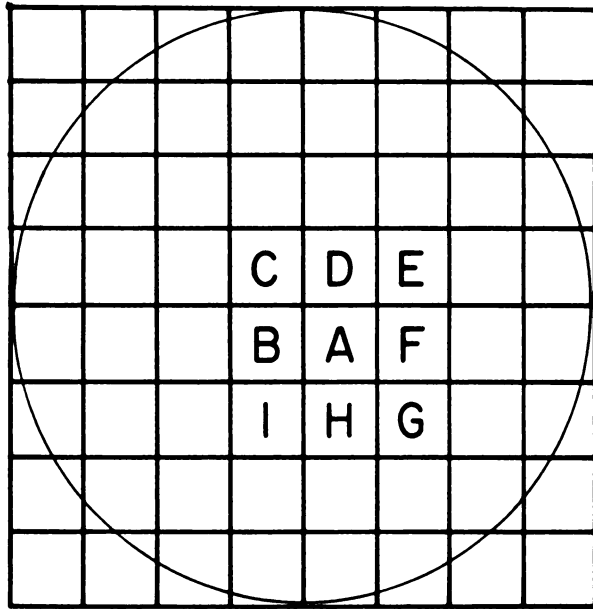


FIG. 3. Circumscribed 8 × 8 matrix superimposed on scintillation crystal. Letters A-I refer to crossover calculations in Table 1.

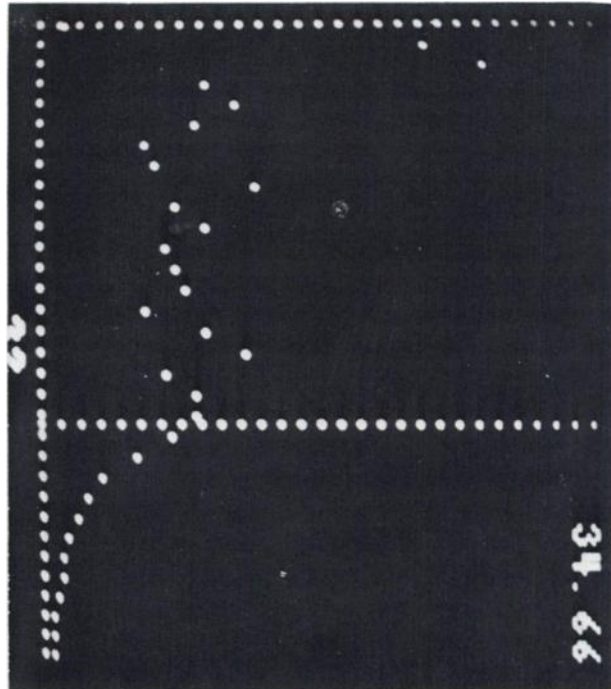


FIG. 4. Oscilloscope display of washout from region over temporal area. First 20 points represent 0.5-sec intervals. Non-nutritional spike (intravascular activity) is seen in first several seconds. Calculated blood flow in cc/min/100 gm is displayed in upper right corner.

averaged out into the early portion of the washout curve and the erroneously high H_{max} would have resulted in an elevated rCBF calculation. By using the short time frames the intravascular spike was isolated in the first ten time frames and was eliminated. The remaining ten 0.5-sec counting rates (from 5 to 10 sec after injection) were averaged to obtain the H_{max} . The area under the activity curve was integrated from 5 sec to 10 min after injection. For each area of data accumulation, the integrated area was divided into $(H_{max} - H_{10})$, where H_{10} is the height at 10 min and multiplied by $\lambda \times 100$. The result was blood flow in cubic centimeters per minute per 100 grams.

After processing, the blood flow measurements were retrieved as a teletype printout representing a composite of the 64 regional blood flows in cubic centimeters per minute per 100 grams and as a CRT display of the individual washout curves with the calculated blood flow for that region (Fig. 4). The printout was arranged in eight columns and eight rows with the position in the printout corresponding to the location in the matrix from which the information was obtained.

RESULTS AND DISCUSSION

Resolution and crossover. We measured the spatial resolution of our system by obtaining a series of line spread functions using a 1.2-mm-i.d. capillary tube filled with ^{133}Xe , a 400-channel analyzer, and the 4,000-hole collimator. The output representing the x-axis pulse was fed into the 512-channel analyzer,

TABLE 1. PERCENT CROSSOVER

Distance from collimator (cm)	Lucite interposed			Lucite + calvarium interposed		
	B/Z	C/Z	X/Z	B/Z	C/Z	X/Z
0	0.93	0.04	3.88	1.43	0.04	5.88
2.5	2.21	0.51	10.88	2.60	0.56	12.64
4.3	3.03	0.74	15.08	3.21	0.84	16.20
6.8	4.41	1.16	22.28	4.8	1.51	25.56
9.0	4.87	1.39	25.04	5.58	1.90	30.92

Letters refer to matrix areas in Fig. 3. A was area covered by ^{133}Xe volume source. B-I were surrounding areas. X was total counts recorded in B-I (adjacent matrices) and Z was total counts recorded in A-I (adjacent plus source matrices). Counting rates in areas outside of Z were insignificant. Consequently, ratio X/Z represented total percent crossover.

and the x-axis was divided into 256 segments for data accumulation. The line source was placed at the collimator surface perpendicular to the x-axis and at 2.5, 4.7, 7.0, and 11.0 cm from the collimator. Lucite (tissue equivalent density) was interposed between the line source and the collimator. The full width at half maximum (FWHM) for the line source was 1.94 cm at the collimator surface, 2.16 cm at 2.5 cm, 2.20 cm at 4.7 cm, 2.42 cm at 7 cm, and 2.86 cm at 11 cm from the collimator.

Crossover is directly proportional to resolution. In the past it has been used to define the overlap

between two adjacent probes. We define crossover with the Anger camera as the percent of activity from a homogeneous plane source within the field of one matrix area but recorded in adjacent areas. The converse is also true. The percent crossover recorded in adjacent matrices from a source overlying a single matrix area equals the percent of activity recorded in a single matrix area which has resulted from crossover from adjacent areas of a homogeneous extended source. These considerations are of considerable importance when crystal splitting techniques are employed with camera systems since crossover dictates the practical limits to the size of the matrix areas. If a substantial percentage of activity in each matrix area is due to crossover from tissue overlying adjacent areas, further reduction in the size of each matrix is pointless.

To measure crossover in our system, we shielded a 3.5×3.5 source of ^{133}Xe on all surfaces but one. The unshielded surface was placed on the 250-keV, 4,000-hole collimator so that it was completely bounded by one matrix area. Activity was measured in this area and in adjacent areas. The total activity in all areas (total counts) was divided into the activity recorded in each adjacent area (percent crossover into that area). Similar measurements were made with the source at various distances from the collimator with Lucite interposed between the source and collimator and with one thickness of calvarium interposed in addition to the Lucite. Crossover beyond the adjacent matrices was small and therefore disregarded. Total crossover ranged from 3.88% at the collimator face to 25.04% 9 cm from the collimator. The addition of the calvarium between the collimator and phantom increased crossover slightly (Fig. 3, Table 1).

Deadtime correction. The deadtime for the computer system was 50 μsec . The camera deadtime for events occurring within the energy window was 5 μsec ; events outside the window setting prolong the deadtime an additional 1.5 μsec . For system deadtimes of 15 μsec it has been shown that for total crystal counting rates up to 40,000 cps, corrected counts did not differ from true counts by more than 5% using the formula

$$C = \frac{C_{om}}{1 - \tau C_o}$$

where C is the corrected counting rate for the matrix element, C_o the observed counting rate for the whole crystal, C_{om} is the observed counting rate for the matrix element, and τ the deadtime for the system (17). The system deadtime for that study was 15 μsec .

The 40,000 cps ceiling represents the total events recorded by the crystal. The maximum counts per

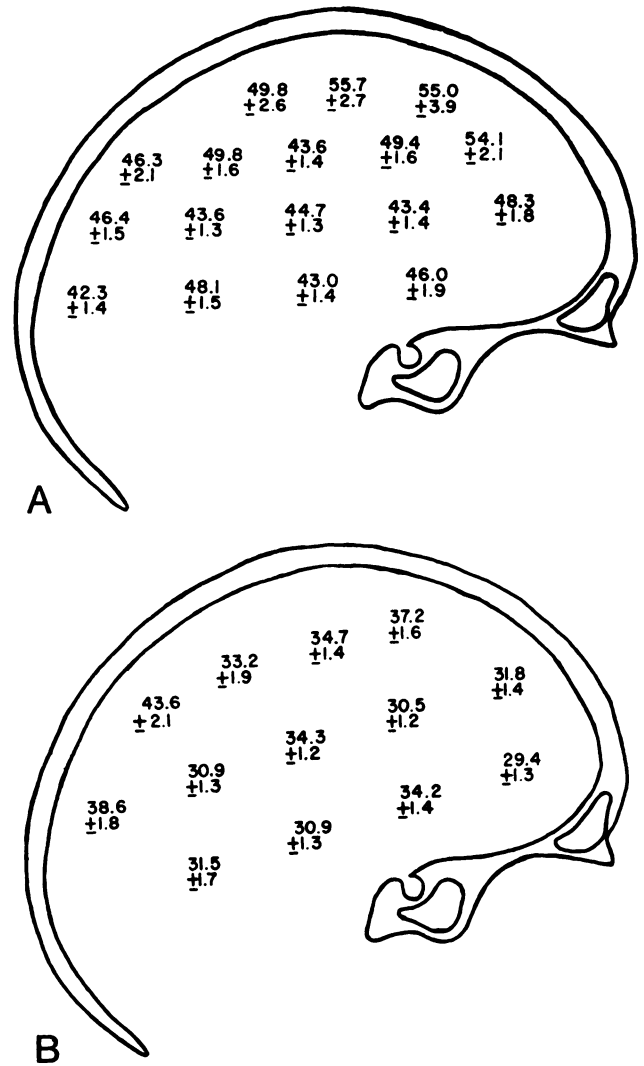


FIG. 5. Regional cerebral blood flow (cc/min/100 gm) before (A) and after (B) hyperventilation (Patient 4) (CBF \pm 1 s.d.).

second within the energy window that can be deadtime corrected is considerably less, particularly with a low-energy nuclide such as ^{133}Xe which is also producing a 31-keV characteristic x-ray and scattered radiation. To determine the maximum number of counts that could be accepted within the energy window with the pulse-height analyzer peaked over the 81-keV photopeak, we placed a volume source ($1 \times 1 \times 1$ cm) containing ^{133}Xe at the collimator face and at varying distances from the collimator with Lucite interposed. We counted the source with a wide open window ($0-\infty$) and with a 25% window (70–90 keV). The ratio of window counts to total counts was 51% at the collimator, 48% at 2.5 cm, 48% at 4.3 cm, 45% at 6.9 cm, and 44% at 9 cm (Table 2). Assuming the worst possible case, a ratio of 44%, counting rates for the entire crystal up to 17,600 cps within the window setting can be deadtime corrected. The maximum counting rate

TABLE 2. RATIO OF WINDOW TO TOTAL COUNTS FOR ^{133}Xe AND A 25% WINDOW

Distance from collimator (Lucite interposed) (cm)	Counting rate in window (total counting rate)
0	51%
2.5	48%
4.3	48%
6.8	45%
9.0	44%

after arterial injection must be accurately estimated beforehand so that counting rates do not exceed the correctable limits. For the five patients studied in this series (7–10 mCi ^{133}Xe), the maximum counting rate ranged from 3,167 to 4,590 cps for the whole crystal, well within the correctable limits.

H_{\max} . We assumed that the time from 5 to 10 sec was a plateau representing the maximum height of the washout curve. To determine the validity of our assumption, we calculated the slopes for this time period for each of the patients studied. The average slope was $-0.0083 \pm 0.0075 \text{ sec}^{-1}$. Since the slope did not deviate significantly from zero, and since the standard deviation was small, we assumed that we were calculating H_{\max} over a plateau and were, therefore, not significantly underestimating rCBF. We also determined H_{\max} from earlier time frames (3–7 sec). The rCBF ranged from 2.66 to 6.63% higher than when H_{\max} was obtained from the 5–10-sec portion of the curve and would have resulted in an average increase in blood flow of 3.61%. However, when the slopes were calculated for the curve between 3 and 7 sec, they ranged from -0.011 to 0.020 sec^{-1} with an average of 0.0143, slightly higher than the slope for the washout between 5 and 10 sec. This probably represented the effect of the intravascular spike. The tail of the spike elevated the counting rate at 3 sec and produced a steeper slope. On visual inspection of the washout curves the peak of the intravascular spike was generally seen between 1 and 2 sec with the tail of the peak extending to 3 sec in several of the patients. Consequently, we employed the 5–10-sec period of the washout curve for the calculation of H_{\max} because it was a plateau unaffected by the intravascular spike.

Statistical analysis. The variance was determined for each variable in the equation

$$F = \frac{H_{\max} - H_{10}}{A} \times \lambda \times 100.$$

Because H_{\max} was determined by summing the 0.5-sec counts from 5 to 10 sec, the standard deviation

TABLE 3. MEAN CEREBRAL BLOOD FLOW

Patient	CBF (cc/min/100 gm) \pm s.d.
1	45.7
2	60.2
3	50.2
4	47.6
5	45.3
mean	50.5 ± 6.2
Normal mean values found by other investigators	
Investigator	CBF (cc/min/100 gm) \pm s.d.
D. Ingvar, et al (Ref. 21)	49.8 ± 5.4
Kety, et al (Ref. 4)	54 ± 12
Lassen, et al (Ref. 20)	52 ± 9

of H_{\max} was equal to $(H_{\max})^{1/2}$, where H_{\max} equals the summated counts from 5 to 10 sec. Similarly, σ of the area is equal to $(A)^{1/2}$, where A is the total number of counts from H_{\max} to H_{10} . For H_{10} , the σ equals $(H_{10})^{1/2}$, where H_{10} is the number of counts recorded in the fortieth time frame (at 10 min). To determine the approximate variance of rCBF values, we applied the standard propagation-of-error formulas

$$\sigma(H_{\max} - H_{10}) = (\sigma^2 H_{\max} + \sigma^2 H_{10})^{1/2},$$

$$\text{RSD}_{\text{CBF}} \cong \left[\left(\frac{\sigma H_{\max} - H_{10}}{H_{\max} - H_{10}} \right)^2 + \left(\frac{\sigma A}{A} \right)^2 \right]^{1/2} = \left[\left(\frac{\sigma H_{\max} - H_{10}}{H_{\max} - H_{10}} \right)^2 + \frac{1}{A} \right]^{1/2},$$

where RSD_{CBF} is the relative standard deviation.

The relative contribution of H_{\max} to RSD_{CBF} is considerably greater than the contribution from the area and H_{10} . For example, in the patient illustrated in Fig. 5, increasing H_{\max} by 1 s.d. affects the regional blood flow measurement 5.31 times more than a similar change in the area and 26.15 times more than an increase of 1 s.d. in H_{10} .

Data analysis. The average blood flows in the five patients studied ranged from 43.3 to 60.2 cc/min/100 gm with a mean of 50.50 cc/min/100 gm. The flows are listed in Table 3 along with values obtained by other investigators in normal subjects (4,20,21).

The regional blood flows in two of our patients are shown in Figs. 5 and 6. The patient in Fig. 5 hyper-ventilated for several minutes after the initial study. His pCO_2 fell from 36 to 25 mmHg and a repeat study was performed. The regional blood flows fell by 28.62% from the initial study (Fig. 5). This is quite close to the predicted decrease in rCBF of about 2.8%/mmHg fall in pCO_2 reported by Reivich (22) which would have resulted in a 32% fall in rCBF.

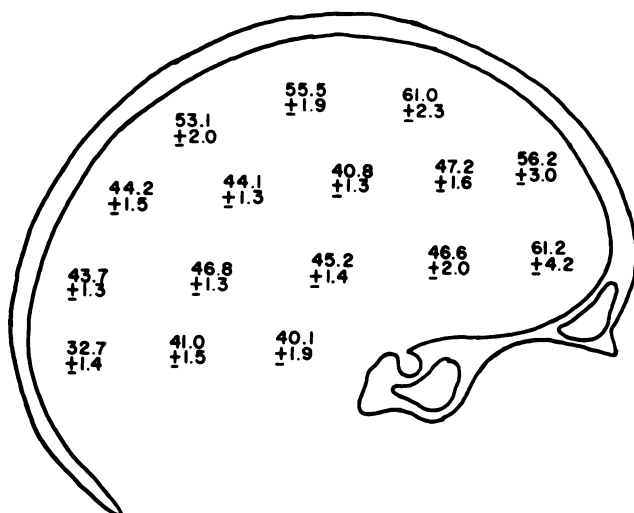


FIG. 6. Regional cerebral blood flow (cc/min/100 gm) ± s.d. in Patient 1.

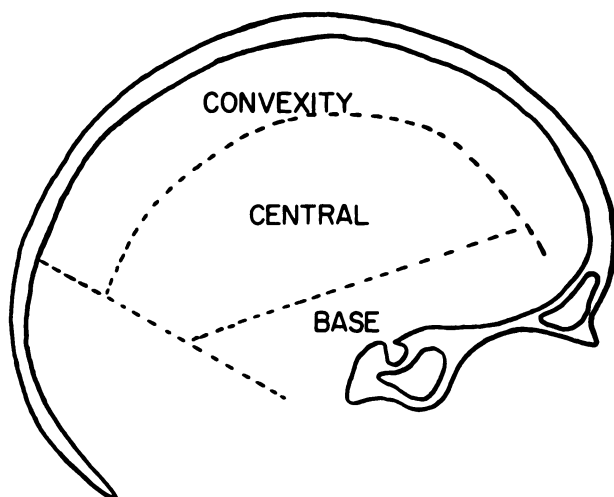


FIG. 7. Comparison of blood flow between areas marked convexity, central, and base (see Table 4).

The data were analyzed for regional variations in blood flow. A significant variation was found between the flow rate over the convexity and that over the midportion and the base of the hemisphere in each patient (Fig. 7, Table 4). The flow over the convexity ranged between 9.9 and 28.0% (an average of 19.3%) higher than the midportion. The base was between 2.7 and 14.1% (an average of 7.1%) lower than the midportion.

To determine whether the regional variations were due to differences in the ratio between fast and slow components (we assumed a constant 60:40 ratio for our λ), we calculated blood flow by compartment analysis and determined the relative weights of the fast and slow compartments for the patient (No. 1)

TABLE 4. REGIONAL DIFFERENCES IN CBF*

Patient	Convexity	Central	Base
1	56.6	44.2	38.0
	↑ 28.1%		↓ 14.1%
2	74.5	61.1	55.4
	↑ 21.7%		↓ 9.4%
3	58.7	49.2	46.3
	↑ 19.3%		↓ 5.9%
4	51.3	46.7	45.4
	↑ 9.9%		↓ 2.7%
5	47.1	40.6	39.3
	↑ 15.9%		↓ 3.4%
Mean	57.6	48.3	44.9
	↑ 19.3%		↓ 7.1%

* Blood flow over convexity, central, and base in five patients and percent increase or decrease from central area. Areas refer to topography illustrated in Fig. 8.

with the greatest difference in regional flows between the midportion and convexity. The ratio of fast to slow components was 54.4:45.6 over the convexity, 49.7:50.3 over the central region, and 51.3:48.7 over the base. These differences would have raised the convexity blood flow by only 3.4% if the values for λ had been corrected for regional alterations in the ratio of fast to slow compartments. Thus even after correcting differences in fast and slow components, the increase in blood flow between regions remains significant.

SUMMARY AND CONCLUSIONS

Regional cerebral blood flow was quantified with the Anger camera after the intra-arterial injection of ¹³³Xe. The camera crystal was electronically divided into an 8 × 8 array and interfaced to a programmed console computer for data accumulation. Stochastic analysis (H/A) was used for calculating the regional blood flows because (A) the computer program is relatively simple and (B) a number of biological assumptions required in compartmental analysis need not be made in stochastic analysis.

Five angiographically normal patients were studied. The average hemispheric flows ranged from 43.3 to 60.2 with a mean of 50.5 cc/min/100 gm. These values are similar to the normal values reported with other techniques.

Regional differences in cerebral blood flow were found in each patient. The flow over the convexity averaged 18.9% higher than the midportion of the hemisphere, and the flow at the base averaged 7.1% lower than the midportion.

The Anger camera is an accurate external detector for measuring regional blood flow with inert gas washout techniques provided that standard dead-time corrections are performed. Stochastic analysis enabled us to use a relatively simple computer pro-

gram so that data could be accumulated and processed on a small general purpose computer. The biological data were similar to that obtained with multiple probes. In addition, regional differences in cerebral blood flow were found with the Anger camera system which have not been described with multiple probe systems.

REFERENCES

1. INGVAR DH, LASSEN NA: Regional cerebral blood flow. *Acta Neurol Scand (Suppl)* 14: 1-97, 1965
2. INGVAR DH, LASSEN NA, SIESJÖ BK, et al: Cerebral blood flow and cerebro-spinal fluid. *Scand J Clin Lab Invest (Suppl)* 102: 1-47, 1968
3. BROCK M, FIESCHE C, INGVAR DH, LASSEN NA, SCHÜRMAN K, eds, Berlin, Springer-Verlag, 1969
4. KETY SS, SCHMIDT CF: The nitrous oxide method for quantitative determination of cerebral blood flow in man: theory, procedure and normal values. *J Clin Invest* 27: 476-492, 1948
5. LASSEN NA, INGVAR DH: The blood flow of the cerebral cortex determined by radioactive krypton-85. *Experimentia* 17: 42-43, 1961
6. LASSEN NA, HOEDT-RASMUSSEN K, SORENSEN SC, et al: Regional cerebral blood flow in man determined by krypton-85. *Neurology* 13: 719-727, 1963
7. ZIERLER KL: Equations for measuring blood flow by external monitoring of radioisotopes. *Circ Res* 16: 309-321, 1965
8. ZIERLER KL: Basic aspects of kinetic theory as applied to tracer-distribution studies. In *Dynamic Clinical Studies with Radioisotopes*, Oak Ridge, Tennessee, USAEC, 1964, pp 55-80
9. MEIER P, ZIERLER KL: On the theory of the indicator-dilution method for measurement of blood flow and volume. *J Appl Physiol* 6: 731-744, 1954
10. LASSEN NA, KLEE A: Cerebral blood flow determined by saturation and desaturation with krypton-85. *Circ Res* 16: 26-32, 1965
11. MCHENRY LC, JAFFE ME, GOLDBERG HI: Evaluation of the rCBF method of Lassen and Ingvar. In *Cerebral Blood Flow: Clinical and Experimental Results*. Brock M, Fieschi C, Ingvar DH, Lassen NA, Schürmann K, eds, Berlin, Springer-Verlag, 1969
12. POTCHEN EJ, DAVID DO, WHARTON T, et al: Regional cerebral blood flow in man: a study of the xenon 133 washout method. *Arch Neurol (Chicago)* 20: 378-383, 1969
13. HOEDT-RASMUSSEN K, SVEINSDOTTIR E, LASSEN NA: Regional cerebral blood flow in man determined by interarterial injection of radioactive inert gas. *Circ Res* 18: 237-249, 1966
14. ROSS RS, UEDA K, LICHTEN PR, et al: Measurement of myocardial blood flow in animals and man by the selective injection of radioactive inert gas into the coronary arteries. *Circ Res* 15: 28-41, 1964
15. VEALL N, MALLETT BL: The partition of trace amounts of xenon between human blood and brain tissues at 37°C. *Phys Med Biol* 10: 375-380, 1965
16. POTCHEN EJ, BENTLEY R, GERTH W, et al: A means for scintigraphic imaging of regional brain dynamics—regional cerebral blood flow and regional cerebral blood volume. In *Medical Radioisotope Scintigraphy*, vol 2, Vienna, IAEA, 1969, pp 577-582
17. COX JR, HILL RL: Interface design considerations. In *Computer Processing of Dynamic Images from an Anger Scintillation Camera*, vol 1, St. Louis, Washington University, 1971, pp 9/1-9/39
18. HILL R, CLIFTON J, GALLAGER T, et al: Regional cerebral blood flow in man: data acquisition and analysis. *Arch Neurol (Chicago)* 20: 384-387, 1969
19. POTCHEN EJ, DAVIS DO, ADATEPE MH, et al: Shunt flow in glioblastoma: study in regional autoregulation. *Invest Radiol* 4: 186-192, 1969
20. LASSEN NA, MUNCK O: The cerebral blood flow in man determined by the use of radioactive krypton. *Acta Physiol Scand* 33: 30-49, 1955
21. INGVAR DH, CRONQVIST S, EKBERG R, et al: Normal values of cerebral blood flow in man, including flow and weight estimates of gray and white matter. *Acta Neurol Scand (Suppl)* 14: 72-78, 1965
22. REIVICH M: Arterial P_{CO₂} and cerebral hemodynamics. *Amer J Physiol* 206: 25-35, 1964